Int. J. Solids Structures Vol. 26, No. 9/10, pp. 993–1004, 1990
Printed in Great Britain.

0020–7683/90 $3.00 + .00

EFFECT OF RESIDUAL STRESSES ON PLASTIC BUCKLING OF CYLINDRICAL SHELL STRUCTURES

KIM RAVN-JENSEN
MAN B&W Diesel A/S, Copenhagen, Denmark

and

VIGGO TVERGAARD
Department of Solid Mechanics, The Technical University of Denmark,
DK-2800 Lyngby, Denmark

Abstract—Weld-induced residual stresses in shell structures tend to give earlier onset of plastic yielding and to reduce the critical buckling load. Geometrical imperfections may also have a detrimental effect on the load carrying capacity. The interaction between these two kinds of imperfections is studied here for various longitudinally welded cylindrical shell structures, with focus on short wave local buckling modes. It is found that structures with reduced bifurcation loads due to residual stresses show less sensitivity to geometrical imperfections, and after buckling mode deflections of the order of the shell thickness, the residual stresses play no role at all.

1. INTRODUCTION

For shell structures subject to compressive loading in the elastic range a very unstable post-buckling behaviour with an associated strong imperfection-sensitivity is often found, both in theoretical and experimental investigations (Koiter, 1945; Budiansky, 1974; Babcock, 1974). This behaviour is entirely dependent on geometric nonlinearities, whereas, in the plastic range, the picture is further complicated by the interaction with material non-linearities.

Bifurcation in the plastic range takes place under increasing load (Shanley, 1947; Hill, 1958; Hill, 1961), but apart from this initial behaviour plasticity tends to have a destabilizing effect (Hutchinson, 1974; Needleman and Tvergaard, 1982). Thus, structural components with a stable elastic post-buckling behaviour, such as columns or plates, tend to show imperfection sensitivity in the plastic range. However, for a complete spherical shell under external pressure or a circular cylindrical shell under axial compression, which are highly imperfection-sensitive structures in the elastic range, the reduction of the load carrying capacity is relatively smaller in the plastic range, for a given ratio of the imperfection amplitude and the shell thickness (Hutchinson, 1972; Tvergaard, 1983).

Residual stresses can significantly lower the elastic buckling load, or even result in buckling without external loading. This is quite analogous to the effect of thermal expansion, which can lead to thermal buckling of nonuniformly heated shells (see the discussion by Bushnell, 1985). For more thick-walled shell structures, where buckling occurs in the plastic range, the influence of residual stresses is mostly related to the earlier onset of plastic yielding with the corresponding loss of stiffness in some parts of the material.

Welding is an important source of residual stresses. Much work has been devoted to studying the effect of weld-induced residual stresses on the buckling of plate structures (Dwight and Moxham, 1969; Graves Smith, 1971; Little, 1977). Also, for an axisymmetric shell under external pressure with internal ring-stiffeners welded to it, the effect of the welds on the buckling pressure has been analyzed (Bushnell, 1985). Cold bending of metal sheets is another process that gives rise to significant residual stresses, which oscillate through the thickness after springback, varying between tension and compression.

The present paper considers the effect of weld-induced residual stresses in shell structures, with the main emphasis on non-axisymmetric cases. First, the basic shell equations and constitutive relations required for the analysis of plastic buckling are presented, and

the representation of well-induced residual stresses is discussed. Then, a computational procedure is given, and the effect of welds is illustrated by results obtained for various cylindrical shell structures (Ravn-Jensen, 1984).

2. SHELL EQUATIONS

A point on the shell middle surface is identified by the coordinates x^α. The displacement components are u^α on the corresponding surface base vectors and w on the surface normal. Greek indices range from 1–2, while Latin indices (to be employed subsequently), range from 1 to 3, and the summation convention is adopted for repeated indices.

The nonlinear membrane strain tensor is

$$\varepsilon_{\alpha\beta} = \tfrac{1}{2}(u_{\alpha,\beta}+u_{\beta,\alpha}) - d_{\alpha\beta}w + \tfrac{1}{2}a^{\gamma\delta}(u_{\gamma,\alpha}-d_{\gamma\alpha}w)(u_{\delta,\beta}-d_{\delta\beta}w) + \tfrac{1}{2}(w_{,\alpha}+d^{\gamma}_{\alpha}u_{\gamma})(w_{,\beta}+d^{\delta}_{\beta}u_{\delta}) \quad (1)$$

and the linear bending strain tensor for the middle surface is used in the form (Niordson, 1985)

$$\kappa_{\alpha\beta} = w_{,\alpha\beta} + d_{\alpha\gamma}u^{\gamma}_{,\beta} + d_{\beta\gamma}u^{\gamma}_{,\alpha} + u^{\gamma}d_{\gamma\alpha,\beta} - d_{\beta\gamma}d^{\gamma}_{\alpha}w. \quad (2)$$

Here, $a_{\alpha\beta}$ and $d_{\alpha\beta}$ are the metric tensor and the curvature tensor, respectively, of the undeformed middle surface, and $(\ )_{,\alpha}$ denotes covariant differentiation. It is noted that (1) and (2) are identical to the strain measures proposed by Koiter (1966), except for small differences in the bending strain measure of the order of $d^{\gamma}_{\alpha}\varepsilon_{\gamma\beta}$.

In cases where two shell segments are bonded to one another along a line, continuity of rotations around this line is required. If n^α is a unit in-plane normal to the line, the angle of rotation ψ around the line is given by

$$\psi = (w_{,\beta} + d^{\delta}_{\beta}u_{\delta})n^{\beta}. \quad (3)$$

The three-dimensional constitutive relations are taken to be of the form

$$\dot{\sigma}^{ij} = L^{ijkl}\dot{\eta}_{kl} \quad (4)$$

where σ^{ij} is the stress tensor, η_{kl} is the strain tensor, L^{ijkl} are the instantaneous moduli, and $\dot{(\ )}$ denotes an incremental quantity. Since the stress state in the shell is approximately plane, only the in-plane stresses enter in (4), and the constitutive relations can be written as

$$\dot{\sigma}^{\alpha\beta} = \hat{L}^{\alpha\beta\gamma\delta}\dot{\eta}_{\gamma\delta}, \quad \hat{L}^{\alpha\beta\gamma\delta} = L^{\alpha\beta\gamma\delta} - \frac{L^{\alpha\beta 33}L^{33\gamma\delta}}{L^{3333}}. \quad (5)$$

The in-plane components of the Lagrangian strain tensor at a distance x^3 from the shell middle surface (x^i is a right-handed coordinate system) are approximated by

$$\eta_{\alpha\beta} = \varepsilon_{\alpha\beta} - x^3\kappa_{\alpha\beta}. \quad (6)$$

The membrane stress tensor $N^{\alpha\beta}$ and the moment tensor $M^{\alpha\beta}$ in a shell with thickness h are taken to be

$$N^{\alpha\beta} = \int_{-h/2}^{h/2} \sigma^{\alpha\beta}\,\mathrm{d}x^3, \quad M^{\alpha\beta} = -\int_{-h/2}^{h/2} \sigma^{\alpha\beta}x^3\,\mathrm{d}x^3. \quad (7)$$

Then, from eqns (5), (6) and (7), incremental relations are obtained for $\dot{N}^{\alpha\beta}$ and $\dot{M}^{\alpha\beta}$ in terms of $\dot{\varepsilon}_{\gamma\delta}$ and $\dot{\kappa}_{\gamma\delta}$. The requirement of equilibrium is specified in terms of the principle of virtual work

$$\int_A \{N^{\alpha\beta}\delta\varepsilon_{\alpha\beta} + M^{\alpha\beta}\delta\kappa_{\alpha\beta}\}\,\mathrm{d}A = \delta W_e \tag{8}$$

where A is the middle surface area, and δW_e is the external virtual work. Expansion of (8) about the current approximate equilibrium state gives to lowest order the following incremental equilibrium equation

$$\int_A \{\dot{N}^{\alpha\beta}\delta\varepsilon_{\alpha\beta} + \dot{M}^{\alpha\beta}\delta\kappa_{\alpha\beta} + N^{\alpha\beta}[a^{\gamma\mu}(\dot{u}_{\gamma,\alpha} - d_{\gamma\alpha}\dot{w})(\delta u_{\mu,\beta} - d_{\mu\beta}\delta w)$$

$$+ (\dot{w}_{,\alpha} + d^{\gamma}_{\alpha}\dot{u}_{\gamma})(\delta w_{,\beta} + d^{\mu}_{\beta}\delta u_{\mu})]\}\,\mathrm{d}A = \delta\dot{W}_e - \left[\int_A \{N^{\alpha\beta}\delta\varepsilon_{\alpha\beta} + M^{\alpha\beta}\delta\kappa_{\alpha\beta}\}\,\mathrm{d}A - \delta W_e\right]. \tag{9}$$

The terms bracketed on the right-hand side of (9) are included to prevent drifting of a numerical solution away from the true equilibrium path.

The theory of plasticity employed here is small-strain J_2-flow theory with isotropic hardening. In the three-dimensional x^i-coordinate system with metric tensor g_{ij} the instantaneous moduli are

$$L^{ijkl} = \frac{E}{1+\nu}\left\{\tfrac{1}{2}(g^{ik}g^{jl} + g^{il}g^{jk}) + \frac{\nu}{1-2\nu}g^{ij}g^{kl} - f\frac{s^{ij}s^{kl}}{\sigma_e^2}\right\} \tag{10}$$

where E and ν are Young's modulus and Poisson's ratio, respectively, $\sigma_e = (3s_{ij}s^{ij}/2)^{1/2}$, in terms of $s^{ij} = \sigma^{ij} - g^{ij}\sigma^k_k/3$, and

$$f(\sigma_e) = \begin{cases} \dfrac{3}{2}\dfrac{E/E_t - 1}{E/E_t - (1-2\nu)/3}, & \text{for } \sigma_e = (\sigma_e)_{\max} \text{ and } \dot{\sigma}_e \geqslant 0 \\ 0, & \text{for } \sigma_e < (\sigma_e)_{\max} \text{ or } \dot{\sigma}_e < 0. \end{cases} \tag{11}$$

The initial value of $(\sigma_e)_{\max}$ is the yield stress σ_y, and the tangent modulus E_t is the slope of the uniaxial stress–strain curve, which is here

$$\varepsilon = \begin{cases} \dfrac{\sigma}{E}, & \text{for } \sigma \leqslant \sigma_y \\ \dfrac{\sigma_y}{E}\left[\dfrac{1}{n}\left(\dfrac{\sigma}{\sigma_y}\right)^n - \dfrac{1}{n} + 1\right], & \text{for } \sigma > \sigma_y \end{cases} \tag{12}$$

with strain hardening exponent n.

3. WELD-INDUCED RESIDUAL STRESSES

When two shell segments are welded together, the material along the weld is heated to the melting temperature, and stress relaxation at the high temperature is so rapid that the heated structure is essentially stress free. However, when the structure is subsequently cooled to room temperature, large tensile stresses develop along the weld as a result of thermal contraction, while compressive stresses develop farther away from the weld to keep equilibrium.

In Fig. 1a the dashed curve indicates a possible idealization of the residual stresses

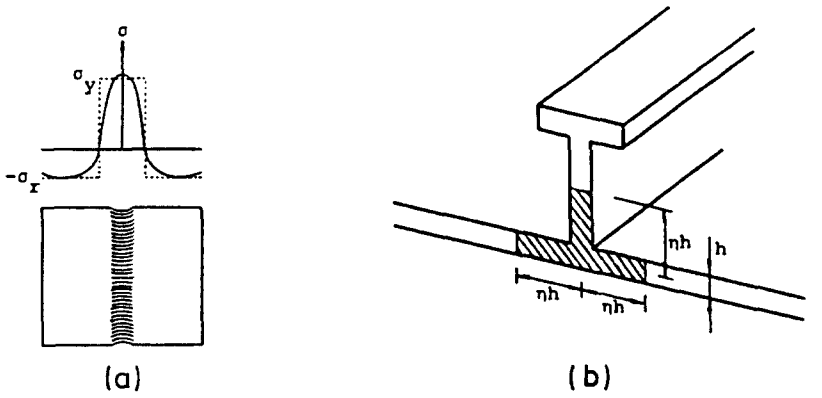

Fig. 1. (a) Residual stress distribution in direction parallel to weld. (b) Hatched region shows tension zone used to model weld-induced residual stresses.

after welding. It is assumed that the tensile stresses are constant and equal to the initial yield stress σ_y in a strip of material near the weld, while the constant compressive stresses σ_r are somewhat smaller than σ_y. This model of the weld-induced residual stresses has been discussed and recommended by Dwight and Moxham (1969), who have also used the model in analyses of welded plate structures. On the basis of empirical investigations, Faulkner (1977) has suggested using a tension zone such as that illustrated by the hatched region in Fig. 1b, where the value of η is between 3 and 6, common for all plate segments meeting at the weld. In examples in the following sections the value σ_r/σ_y will be specified; but it is noted that indirectly this gives the value of η, since the tensile residual stresses are taken to be σ_y.

For perfectly flat plates welded together the assumed residual stress field can satisfy equilibrium accurately, and the same is true for uniformly spaced welds in the longitudinal direction of a cylindrical shell. However, in the case of circumferential welds in cylindrical shells, or in cases where the plate or shell segments to be welded have initial geometrical imperfections, the assumed uniform residual stress fields do not satisfy equilibrium directly. In such cases the actual initial geometry and stress fields are calculated numerically by a few initial increments, which may incorporate a small amount of plastic yielding, since the material in the tensile zones starts out on the yield surface. This incremental determination of the initial equilibrium state is important here, since a number of the calculations to be discussed focus on the interaction of geometrical imperfections and weld-induced residual stresses. It is noted that during these initial increments the general features of the residual stress distribution remain as shown in Fig. 1a.

4. SOLUTION METHOD

The computational results to be considered here refer to cylindrical shell structures, welded along lines parallel with the cylinder axis. Initial imperfections are taken to be periodic in the axial direction with a certain wavelength L, and the solutions are restricted to buckling patterns that remain periodic with the same wavelength L. The middle surface coordinates are taken to have x^1 in the axial direction and x^2 in the circumferential direction. Then, for arbitrary cross-sectional shapes of the cylindrical shells the displacement components can be expressed by a series expansion in axial direction

$$\begin{Bmatrix} u^1 \\ u^2 \\ w \end{Bmatrix} = \begin{Bmatrix} U_0^1(x^2)\dfrac{x^1}{L} \\ U_0^2(x^2) \\ W_0(x^2) \end{Bmatrix} + \sum_{n=1}^{N} \begin{Bmatrix} U_n^1(x^2)\cos\dfrac{2\pi n x^1}{L} \\ U_n^2(x^2)\sin\dfrac{2\pi n x^1}{L} \\ W_n(x^2)\sin\dfrac{2\pi n x^1}{L} \end{Bmatrix} \tag{13}$$

as has been suggested by Tvergaard (1978) for oval cylindrical shells. In the incremental finite element solution based on (9) the one-dimensional amplitude functions U_n^1, U_n^2 and W_n are approximated by Hermitian cubics within each element.

In the expansion (13) it has been found that using $N = 2$ gives good accuracy. The integrals in (9) are evaluated by four-point Gaussian quadrature in circumferential direction within each element, while eight-point Gausssian integration is used in the axial direction, within the interval $[-L/4, L/4]$. Through the thickness Simpson's rule is used, with seven points in (7). The active branch of the tensor of instantaneous moduli (10) is determined in each integration point, according to whether elastic unloading or plastic loading took place in the previous increment [see eqn (11)].

Buckling of a geometrically perfect shell initiates at a bifurcation point. The bifurcation load and the corresponding bifurcation mode are determined by application of Hill (1958) and Hill (1961) general theory for uniqueness and bifurcation in elastic–plastic solids. The details of this analysis shall not be discussed here [e.g. see Hutchinson (1974) or Needleman and Tvergaard (1982)]; but it is noted that the bifurcation mode is of the form (13), with a certain critical wavelength L_c and corresponding amplitude functions $\tilde{U}_1^1$, $\tilde{U}_1^2$, $\tilde{W}_1$. Such bifurcation analyses have been carried out for each of the shell structures to be discussed in the following, both in the initially stress-free cases and in the cases with weld-induced residual stresses. When initial geometrical imperfections with amplitude ξ are specified, these imperfections are taken to be in the shape of the first critical bifurcation mode for the corresponding perfect structure (although sometimes a wavelength L different from L_c is applied), with ξ denoting the maximum normal deflection $\tilde{W}_1$ normalized by the shell thickness.

It is well known that bifurcation calculations based on the deformation theory of plasticity generally agree better with experimental buckling loads for plate and shell structures than similar calculations based on J_2 flow theory. Bifurcation predictions of deformation theory can be justified by appealing to a more sophisticated flow theory, where a vertex forms on the yield surface (Hutchinson, 1974; Needleman and Tvergaard, 1982). The application of such a corner theory of plasticity can also be significant for initially imperfect shells, particularly in cases where second bifurcations occur (Tvergaard, 1983). However, the discrepancies between bifurcation predictions based on different constitutive laws are small as long as the initial yield stress is only slightly exceeded, and therefore it is assumed in the present paper that the material behaviour is reasonably well described by J_2 flow theory.

5. RESULTS FOR CYLINDRICAL SHELL STRUCTURES

For a longitudinally stiffened circular cylindrical shell under axial compression local buckling of the shell between the stiffeners is the first critical bifurcation mode, provided that the stiffeners are sufficiently strong. Such buckling in a short wave pattern between the stiffeners has been analysed by Koiter (1956) for elastic shells and by Tvergaard (1977) for elastic–plastic shells. Here, the additional effect of the residual stresses induced by welding the stiffeners onto the shell will be studied.

The stiffener spacing, measured along the shell middle surface, is denoted by b, and the shell material is taken to have $\sigma_y/E = 0.002$, $\nu = 0.3$ and a strain-hardening exponent n to be specified for each case. As in previous analyses for axially compressed cylindrical panels (Koiter, 1956; Tvergaard, 1977), the stiffeners are assumed sufficiently strong to prevent waviness of radial deflections along their lines of attachment, while all other effects of the stiffeners are neglected. Thus, the actual stiffener geometry and the stress distribution inside the stiffeners are not accounted for in the results to be presented here. It is noted that computations have been carried out for plates reinforced by T-stiffeners with the cross-sectional height $0.2b$ and the width $0.1b$ of the top flange (Ravn-Jensen, 1984), and the plate results for idealized stiffeners to be presented here differ only little from those based on detailed modelling of T-stiffeners by plate elements.

First, a longitudinally stiffened flat plate is considered, for which Fig. 2 illustrates the local buckling mode investigated. Due to various symmetries only one quarter of the region shown in Fig. 2 needs to be analyzed numerically. The discretization in the longitudinal

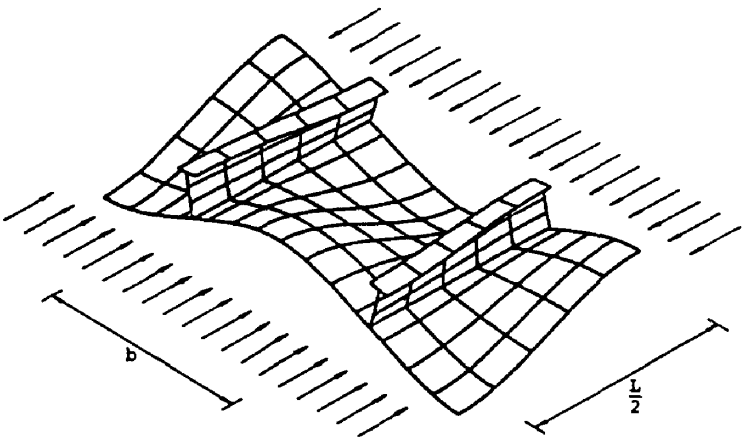

Fig. 2. Local buckling mode analyzed for longitudinally stiffened plates under axial compression.

direction is based on using $N = 2$ in (13). In the transverse direction the half-width between two stiffeners is divided into three elements, one inside the residual tensile stress zone and the others outside.

Load deflection curves are shown in Fig. 3 for a panel with $b/h = 40$, made of a low hardening material, $n = 100$. Here the wavelength $L = 1.65b$ is used, which gives slightly lower maximum load carrying capacity for geometrically imperfect panels than the somewhat larger wavelength of the first critical bifurcation mode. The load parameter λ denotes the ratio of the average compressive stress in the panel and the initial yield stress σ_y, while $\underline{w}$ denotes the maximum absolute value of the function $W_1(x^2)$ in (13). Curves are shown for three different levels of the residual compressive stress, $\sigma_r = 0$, $\sigma_r = 0.2\sigma_y$, $\sigma_r = 0.4\sigma_y$, and for each case three different values of the initial geometrical imperfection amplitude are considered, $\xi = 0$, $\xi = 0.01$ and $\xi = 0.1$. The bifurcation load has been determined for the three cases of zero imperfection, and it is seen that bifurcation occurs shortly after the first onset of plastic yielding (indicated by a circle on the curves). In each case the post-bifurcation behaviour is computed as the behaviour of a structure with a very small initial geometrical imperfection ($\xi = 0.0002$).

It is seen in Fig. 3 that the residual stress gives a significant reduction of the bifurcation load. However, the lower bifurcation point has a stable post-bifurcation behaviour, so that part of the reduction in load carrying capacity indicated by the lower bifurcation point is

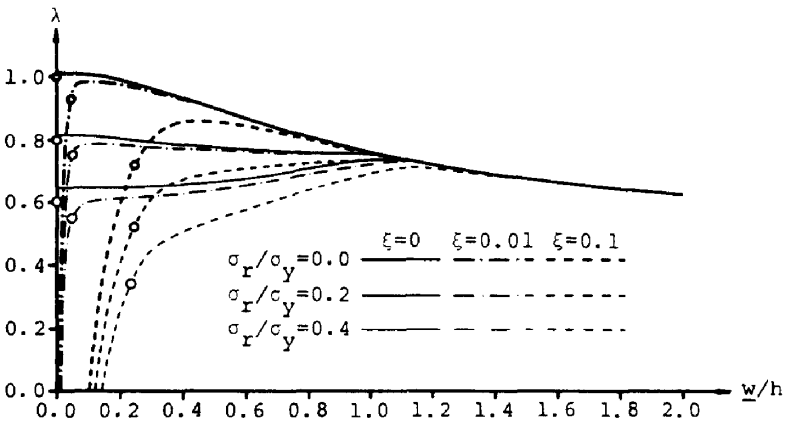

Fig. 3. Load vs local buckling mode deflection for longitudinally stiffened plate with $b/h = 40$ and $n = 100$.

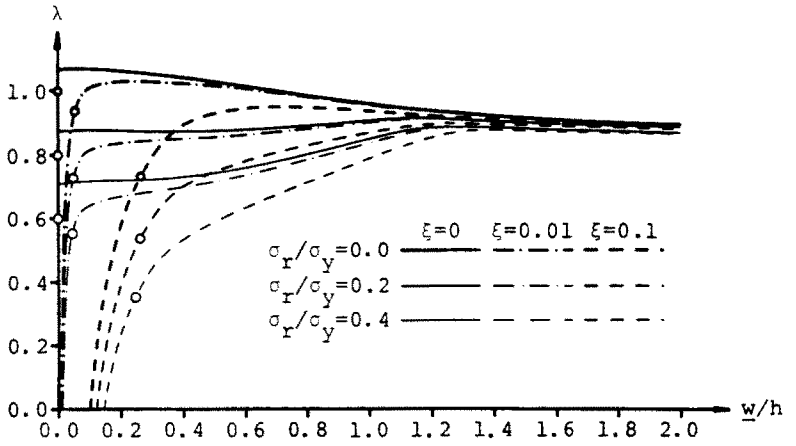

Fig. 4. Load vs local buckling mode deflection for longitudinally stiffened plate with $b/h = 40$ and $n = 10$.

regained through less sensitivity to geometrical imperfections. The most significant feature of the curves in Fig. 3 is that they all meet at $\underline{w} \simeq 1.1h$. Thus, at deflections larger than about a shell thickness, there is no longer any visible effect of the weld-induced residual stresses on the load carrying capacity. In conclusion, both residual stresses and geometrical imperfections can lead to a reduction in the load carrying capacity; but the effect of these two different kinds of imperfections is not additive.

Figure 4 shows similar results for an eccentrically stiffened plate made of a more high-hardening material with $n = 10$. Here, the wavelength L is chosen as that corresponding to the minimum bifurcation load. The behaviour is rather similar to that shown in Fig. 3, but clearly the reductions of the load carrying capacity due to either residual stresses or geometrical imperfections are larger for the low-hardening material in Fig. 3.

It should be emphasized that the local buckling in a short wave pattern between the stiffeners is only one of the possible buckling modes. Other buckling modes involve significant bending of the stiffeners, and nonlinear interaction between different buckling modes can be a significant effect. Thus, for eccentrically stiffened elastic–plastic plates as those shown in Fig. 2, with uniformly spaced transverse supports, Tvergaard and Needleman (1975) have considered the interaction between local buckling mode and a wide column type buckling mode.

Results for a circular cylindrical shell with longitudinal stiffeners are shown in Fig. 5. As in the previous figures the shell is under axial compression, and only local buckling

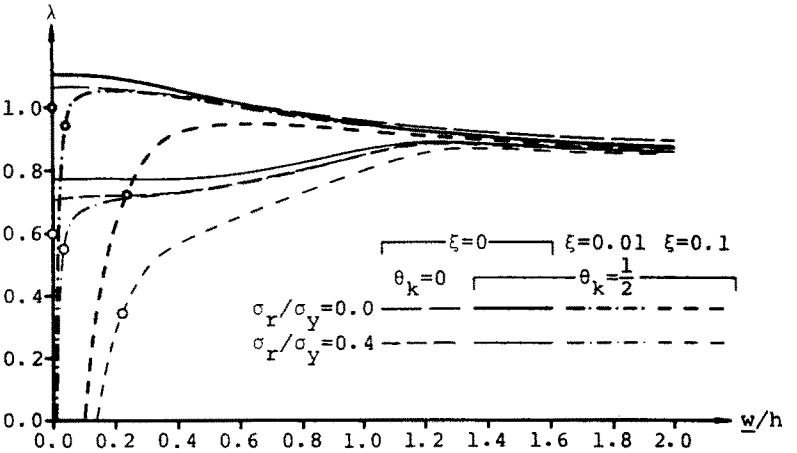

Fig. 5. Load vs local buckling mode deflection for longitudinally stiffened circular cylindrical shell with $\theta_k = 1/2$, $b/h = 40$ and $n = 10$. Plate results ($\theta_k = 0$) shown for comparison.

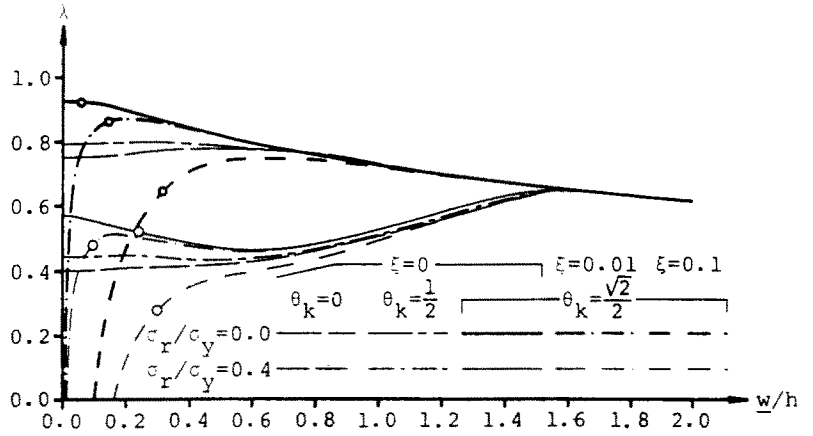

Fig. 6. Load vs local buckling mode deflection for longitudinally stiffened circular cylindrical shell with $\theta_k = \sqrt{2}/2$, $b/h = 50$ and $n = 100$. Results for plate ($\theta_k = 0$) and less curved shell ($\theta_k = 1/2$) shown for comparison.

between the stiffeners is considered (analogous to the mode illustrated in Fig. 2). Also here the spacing to thickness ratio is $b/h = 40$, and the shell curvature $\theta_k = 1/2$ is specified in terms of the curvature measure

$$\theta_k = \frac{\sqrt[4]{12(1-\nu^2)}}{2\pi}\frac{b}{\sqrt{Rh}} \tag{14}$$

introduced by Koiter (1956). Here, R is the radius of the circular cylindrical shell, and the value $\theta_k = 1/2$ in Fig. 5 corresponds to $R/b = 13.4$. For elastic shells with idealized stiffeners it was found by Koiter (1956) that the local buckling mode is unique in the range $0 \leqslant \theta_k \leqslant 1$, whereas for elastic–plastic shells this uniqueness is lost at values of θ_k somewhat smaller than unity (Tvergaard, 1977).

The load deflection curves in Fig. 5 are obtained for the high-hardening material, $n = 10$. Two curves for a flat plate with no geometrical imperfection ($\theta_k = 0$, $\xi = 0$) are included for comparison (taken from Fig. 4). It is seen that the main effect of the curvature ($\theta_k = 1/2$) is to increase the bifurcation loads and the load carrying capacity for small geometrical imperfections, while at $\underline{w} \simeq 1.2h$, where all the curves meet, there is hardly any difference from the stiffened plate results.

Figure 6 shows results for a stiffened shell with $b/h = 50$, made of the low-hardening material, $n = 100$. Here, results are shown for a higher curvature $\theta_k = \sqrt{2}/2$, using the wavelength $L = 1.65b$, and post-bifurcation curves for $\theta_k = 1/2$ and $\theta_k = 0$ are included for comparison. In this case, all bifurcation points occur in the elastic range; but soon after bifurcation plastic yielding sets in, and subsequently the behaviour is much like that found in the previous three figures. It is noted that Fig. 6 represents a case where elastic bifurcation loads are significantly reduced by the residual stresses $\sigma_r/\sigma_y = 0.4$. Furthermore, the slightly higher curvature $\theta_k = \sqrt{2}/2$ gives quite a big increase of the bifurcation loads, with a corresponding increased imperfection-sensitivity.

Load vs axial compression curves are shown in Fig. 7 corresponding to each of the post-bifurcation curves ($\xi = 0$) given in Fig. 6. Here, δ denotes the average axial compressive strain, so that $(E/\sigma_y)\delta = 1$ would signify the onset of plastic yielding in a uniaxial compressive test. The curves for the most curved panel ($\theta_k = \sqrt{2}/2$) show the characteristic unstable initial post-bifurcation behaviour, whereas the plate solutions ($\theta_k = 0$) are initially stable.

It has been found that the simplified Donnell–Mushtari–Vlasov shell equations are in fact adequate for the analysis of the cylindrical panels discussed above, since here the wavelength of the deformation pattern is small compared to the radius of curvature.

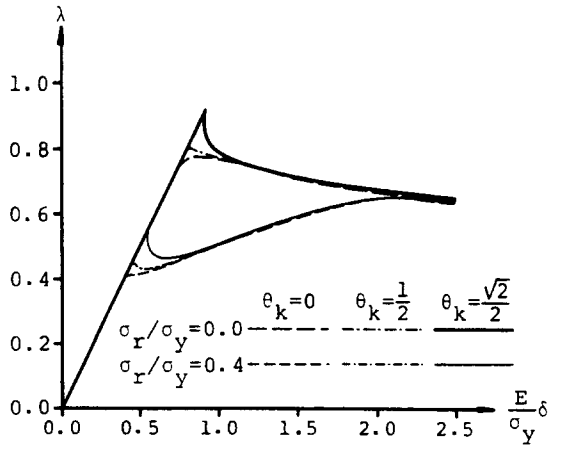

Fig. 7. Load vs axial compression curves for plate ($\theta_k = 0$) and shells ($\theta_k = 1/2$ and $\theta_k = \sqrt{2}/2$), with $b/h = 50$, $n = 100$ and $\xi = 0$.

However, the more accurate first-order shell theory specified by (1)–(3) and (9) is needed for the next cases to be discussed.

Cylindrical shells built up of plates and circular cylindrical shell segments have been analyzed by Almroth and Brogan (1972), who studied elastic buckling behaviour. For a cylindrical shell structure of this type, subject to axial compression, the local buckling behaviour in the plastic range is investigated here. A circular cylindrical shell with radius R is cut along a diameter plane; then the two halves are separated by the distance $2R$ and welded together with two plate strips of width $b = 2R$, to form an oval cylindrical shell with the shape illustrated in Fig. 8a. The tensile residual stresses occur in narrow regions along the four welds, with corresponding compressive stresses σ_r in the remaining part of the shell.

The first critical bifurcation mode (Fig. 8b) involves mainly buckling of the flat plates, and the critical stress is close to that of simply supported plate strips with width $b = 2R$. However, the buckled plate segments lose their stiffness, which leads to a rapid stress redistribution. Consequently, plasticity and buckling deflections quickly spread into the curved parts of the shell, analogous to the behaviour found previously for elastic–plastic cylindrical shells with elliptic cross-section (Tvergaard, 1978). Only the mode which is symmetric about both planes of symmetry of the cross-section (Fig. 8b) is considered here, so that only a region corresponding to one-quarter of the shell circumference and one-half the wavelength in axial direction needs to be analyzed numerically. The half of the plate-segment is divided into three elements (in circumferential direction), with one of these modelling half the weld region, and the 90° circular cylindrical shell segment is divided into four elements, with one modelling half the weld region.

Figure 9 shows load deflection curves for shells with the constant thickness $h = b/40$. The results in Fig. 9a are obtained for the more high-hardening material, $n = 10$, using $L = 1.8b$, while Fig. 9b is obtained for $n = 100$, using $L = 1.65b$. It is seen that the more high-hardening shell shows essentially no imperfection-sensitivity, whereas the low-hardening shell is imperfection-sensitive, due to a stronger effect of the rapid stress redistribution after the onset of plate buckling. As in the above results for stiffened circular cylindrical shells it is noted that the weld-induced residual stresses, $\sigma_r/\sigma_y = 0.2$, significantly reduce the bifurcation load. Also for the oval shells of Fig. 9 it is found that all the curves meet at a certain buckling mode deflection, so that any effect of the residual stresses disappears for deflections larger than $\underline{w} \simeq 1.3h$.

6. CONCLUDING REMARKS

The effect of residual stresses on the buckling behaviour of shell structures has been discussed here with main emphasis on weld-induced residual stresses. The general non-linear field equations for the analysis of any elastic–plastic shell buckling problem have

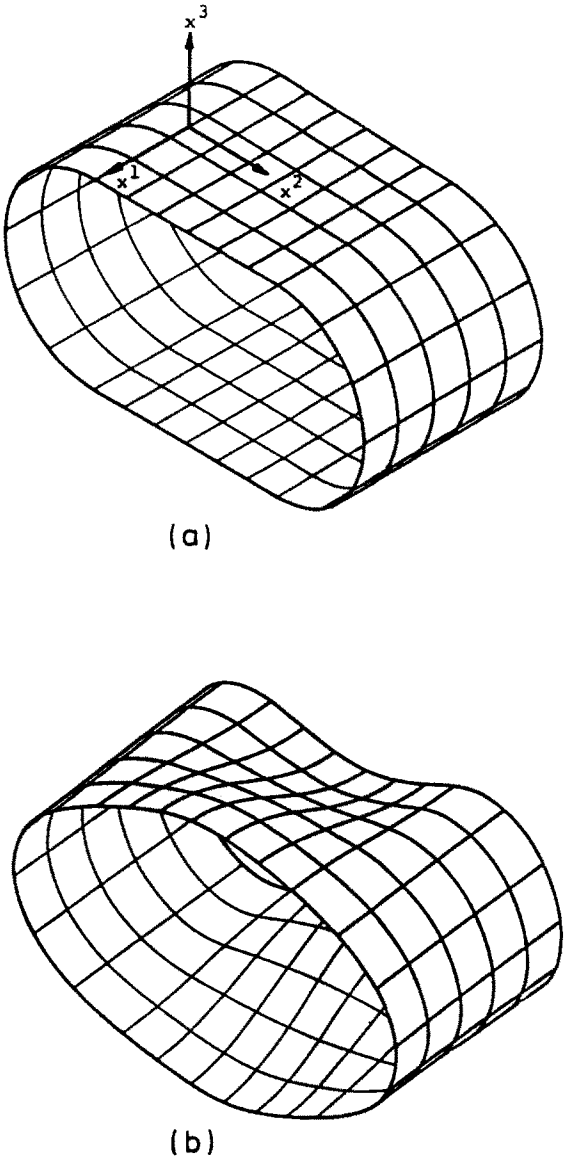

Fig. 8. Oval cylindrical shell built-up from two half circular cylindrical shells and two plates. (a) Shape of the shell. (b) Symmetric short-wave buckling mode analyzed.

been specified, including a procedure for the approximate representation of initial residual stresses; but the examples used to illustrate the buckling behaviour are limited to short wave modes in cylindrical shell structures.

Some characteristic features of the solutions are common for the local buckling between longitudinal stiffeners and the buckling of built-up oval cylindrical shells considered here. Thus, residual stresses reduce the bifurcation loads for geometrically perfect structures; but simultaneously the sensitivity to geometrical imperfections is also reduced. Furthermore, the effect of residual stresses on the load carrying capacity disappears when the buckling mode deflection has reached a certain value of the order of the shell thickness. The general picture is that weld-induced residual stresses reduce the maximum load carrying capacity if the structure is imperfection-sensitive in the absence of residual stresses; but the detrimental effects of residual stresses and geometrical imperfections are not additive.

A complete understanding of the influence of residual stresses on shell buckling behaviour will require much more work. Long wave buckling modes such as column type modes for the whole structure or modes involving significant stiffener bending could show a

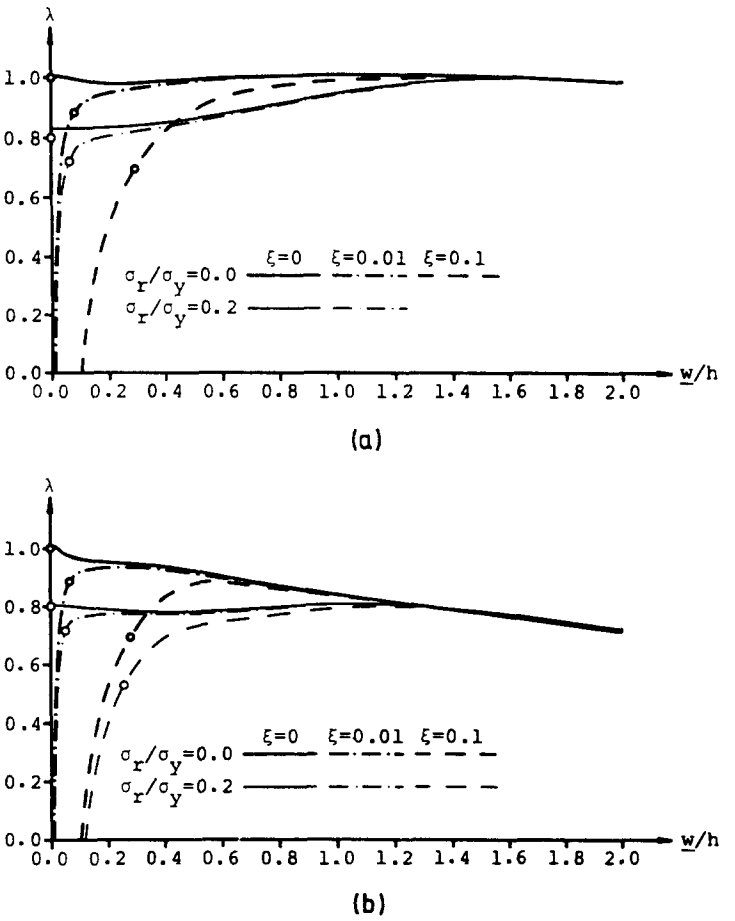

Fig. 9. Load vs short-wave buckling mode deflection for oval cylindrical shells with $b/h = 40$ and $b/R = 2$. (a) $n = 10$, (b) $n = 100$.

different type of response, and also the non-linear interaction between different types of modes would have to be considered.

REFERENCES

Almroth, B. O. and Brogan, F. A. (1972). Bifurcation buckling as an approximation of the collapse load for general shells. *AIAA Jl* **10**, 463–467.

Babcock, C. D. (1974). Experiments in shell buckling. In *Thin Shell Structures* (Edited by Y. C. Fung and E. E. Sechler), pp. 345–369. Prentice-Hall, Englewood Cliffs, NJ.

Budiansky, B. (1974). Theory of buckling and post-buckling behaviour of elastic structures. *Adv. Appl. Mech.* **14**, 1–65.

Bushnell, D. (1985). *Computerized Buckling Analysis of Shells*. Martinus Nijhoff, Dordrecht.

Dwight, J. B. and Moxham, K. E. (1969). Welded steel plates in compression. *Structural Engineer* **47**, 49–66.

Faulkner, D. (1977). Effects of residual stresses on the ductile strength of plane welded grillages and of ring stiffened cylinders. *J. Strain Analysis for Engng Design* **12**, 130–139.

Hill, R. (1958). A general theory of uniqueness and stability in elastic–plastic solids. *J. Mech. Phys. Solids* **6**, 236–249.

Hill, R. (1961). Bifurcation and uniqueness in nonlinear mechanics of continua. In *Problems of Continuum Mechanics*, pp. 155–164. Soc. Ind. Appl. Math., Philadelphia, PA.

Hutchinson, J. W. (1974). Plastic buckling. *Adv. Appl. Mech.* **14**, 67–144.

Hutchinson, J. W. (1972). On the post-buckling behaviour of imperfection-sensitive structures in the plastic range. *J. Appl. Mech.* **39**, 155–162.

Koiter, W. T. (1945). Over de stabiliteit van het elastisch evenwicht. Thesis, Delft, H.J. Paris, Amsterdam. English translations (a) NASA TT-F10, 833 (1967); (b) AFFDL-TR-70-25 (1970).

Koiter, W. T. (1966). On the nonlinear theory of thin elastic shells. *Proc. Kon. Ned. Akad. Wetensch.*, Ser. *B*69, 1–54.

Koiter, W. T. (1956). Buckling and post-buckling behaviour of a cylindrical panel under axial compression. Nationaal Luchtvaart Laboratorium **20,** Report S476, Amsterdam.

Little, G. H. (1977). Rapid analysis of plate collapse by live-energy minimization. *Int. J. Mech. Sci.* **19,** 725–744.

Needleman, A. and Tvergaard, V. (1982). Aspects of plastic post-buckling behaviour. In *Mechanics of Solids*, The Rodney Hill 60th Anniversary Volume (Edited by H. G. Hopkins and M. J. Sewell), pp. 453–498. Pergamon Press, Oxford.

Niordson, F. I. (1985). *Shell Theory*. North-Holland, Amsterdam.

Ravn-Jensen, K. (1984). Influence of residual stresses on the stability of plate- and shell-structures (in Danish). Thesis, Department of Solid Mechanics, Technical Univ. of Denmark.

Shanley, F. R. (1947). Inelastic column theory. *J. Aeronaut. Sci.* **14,** 261–267.

Graves Smith, T. R. (1971). The effect of initial imperfections on the strength of thin-walled box columns. *Int. J. Mech. Sci.* **13,** 911–925.

Tvergaard, V. (1983). Plastic buckling of axially compressed circular cylindrical shells. *Int. J. Thin-Walled Struct.* **1,** 139–163.

Tvergaard, V. (1978). Buckling of elastic–plastic oval cylindrical shells under axial compression. *Int. J. Solids Structures* **12,** 683–691. Errata. *Int. J. Solids Structures* **14,** 329.

Tvergaard, V. (1977). Buckling of elastic–plastic cylindrical panel under axial compression. *Int. J. Solids Structures* **13,** 957–970.

Tvergaard, V. and Needleman, A. (1975). Buckling of eccentrically stiffened elastic–plastic panels on two simple supports or multiply supported. *Int. J. Solids Structures* **11,** 647–663.